Optimal control based dynamics exploration of a rigid car with load transfer

Alessandro Rucco Giuseppe Notarstefano John Hauser

Abstract

In this paper we provide optimal control based strategies to explore the dynamic capabilities of a single-track rigid car which includes tire models and load transfer. Using an explicit formulation of the holonomic constraints imposed on the unconstrained rigid car, we design a car model which includes load transfer without adding suspension models. With this model in hand, we perform an analysis of the equilibrium manifold of the vehicle. That is, we design a continuation and predictor-corrector numerical strategy to compute cornering equilibria on the entire range of operation of the tires. Finally, as main contribution of the paper, we explore the system dynamics by use of novel nonlinear optimal control techniques. The proposed strategies allow to compute aggressive car trajectories and study how the vehicle behaves depending on its parameters. To show the effectiveness of the proposed strategies we compute aggressive maneuvers of the vehicle inspired to testing maneuvers from virtual and real prototyping.

I. INTRODUCTION

A new emerging concept in vehicle design and development is the use of *virtual vehicles*, i.e., software tools that reproduce the behavior of the real vehicle with high fidelity [2], [3]. This allows to perform dynamic tests before developing the real prototype, thus reducing costs and time to market. This engineering area is called *virtual prototyping*.

In order to explore the dynamic capabilities of a car vehicle or to design control strategies to drive it, it is necessary to develop dynamic models that capture interesting dynamic behaviors and, at the same time, can be described by ordinary differential equations of reasonable complexity. Many models have been introduced in the literature to describe the motion of a car vehicle both for simulation and control. Starting from the simplified bicycle model, higher complexity models can be designed by adding different car subsystems such as tires, suspensions, the transmission system, the differential and the engine [4], [5], [6], [7], [8]. The bicycle model is a planar rigid

model that approximates the vehicle as a rigid body with two wheels. It is widely used in the literature since it captures many interesting phenomena concisely. However, this model does not capture some important dynamic effects. One of them is load transfer. The most natural way to model load transfer would be to add suspension models. Using an idea independently developed in [9], see also [10], we will model tire normal loads by means of the reaction forces generated at the vehicle contact points by the ground. This allows to model load transfer without adding suspension models, thus with a reasonable increase in the model complexity.

Car dynamics analysis at maximum performance has been widely investigated in the literature. We provide an overview of the relevant literature for our work. First, an analysis of the equilibrium manifold for race vehicles is performed in [11] and [10]. In particular, existence and stability of "cornering equilibria", i.e. steady-state aggressive turning maneuvers, and bifurcation phenomena are investigated in these papers and references therein. Aggressive non-steady state cornering maneuvers for a rally vehicle were proposed in [9] (see also [12]), and [13]. In [9] trajectories comparable with real testing driver maneuver were obtained by solving a suitable minimum-time optimal control problem, whereas in [13] stability and agility of these maneuvers were studied. In [14] minimum-time trajectories of formula one cars were designed by means of numerical techniques based on nonlinear programming. In [15] and [16] the influence of the vehicle mass and center of mass on minimum-time trajectories was studied. Recently, in [17] a constrained optimal control approach is pursued for optimal trajectory planning in a constrained corridor. A Model Predictive Control approach is used to control the vehicle along the planned trajectory. Model Predictive Control for car vehicles has been widely investigated, see, e.g., [18] and [19]. It is worth noting that the optimal control strategy proposed in the paper for trajectory exploration can be also used in a Model Predictive Control scheme to track a desired curve.

The contributions of the paper are as follows. First, we develop a single-track model of rigid car that extends the capabilities of the well known bicycle model and generalizes the one introduced in [9]. We call this model LT-CAR, where "LT" stands for load transfer. Our LT-CAR model differs from the one in [9] for an additional term in the normal forces that depends on the square of the yaw-rate. Also, we provide a rigorous derivation of the proposed model by use of a Lagrangian approach. Namely, using an explicit formulation of the holonomic constraints imposed on the rigid model, we are able to model the load transfer of the car without modeling the suspensions. The LT-CAR model can be seen as the limit of a model with suspensions whose stiffness goes to infinity. A preliminary version of this mathematical idea was proposed for a rigid motorcycle model in [20], see also [21].

Second, with this model in hand, we perform an analysis of the equilibrium manifold of the vehicle. Namely, we study the set of cornering equilibria, i.e. trajectories of the system that can be performed by use of constant inputs. We design a numerical strategy based on zero finding techniques combined with predictor-corrector continuation methods [22] to compute the equilibrium manifold on the entire range of operation of the tires and parametrize it with respect to the lateral acceleration and the velocity of the vehicle. We show slices of the equilibrium manifold for a saloon car and a sports car with respectively front-wheel and rear-wheel drive transmissions, [23]. Moreover, we investigate the structure of the equilibrium manifold with respect to variations in the horizontal position of the

center of mass. Moving the center of mass from the rear to the front causes a significant change in the structure of the equilibrium manifold giving rise to interesting bifurcations.

Third and final, we develop a trajectory exploration strategy, based on novel nonlinear optimal control techniques introduced in [24], see also [25], and show its effectiveness in understanding complex car trajectories on two testing maneuvers. In the first test, we perform an aggressive maneuver by using a multi-body software, Adams, to generate the desired curve. The objective of this choice is twofold: (i) we show the effectiveness of the exploration strategy in finding an LT-CAR trajectory close to the desired curve, and (ii) we validate the LT-CAR model by showing that the desired curve, which is a trajectory of the full Adams model, is in fact "almost" a trajectory of the LT-CAR model. In the second test, we perform a constant speed maneuver on a real testing track (a typical maneuver for real vehicle testing). We show how to design a full state-input desired curve (from the assigned path and speed) by use of a quasi-static approximation and compute an optimal trajectory that shows a typical driver behavior in shaping the path to keep the speed constant.

The rest of the paper is organized as follows. In Section II we introduce and develop the car model. In Section III we characterize the equilibrium manifold of the car and provide a comparison between two significant choices of the car parameters. Finally, in Section IV we describe the strategy for trajectory exploration and provide numerical computations performed on a virtual track and a real racing track.

II. LT-CAR MODEL DEVELOPMENT

In this section we introduce the car model with load transfer (LT-CAR) studied in the paper. This model is an extension of the one proposed in [9], [10]. We model the car as a single planar rigid body with five degrees of freedom (three displacements and two rotations) and then constrain it to move in a plane (three degrees of freedom) interacting with the road at two body-fixed contact points. The center of mass and the two contact points all lie within a plane with the center of mass located at distance b from the rear contact point and a from the front one, respectively. Each contact-point/road-plane interaction is modeled using a *Pacejka*'s tire model [26]. A planar view of the rigid car model is shown in Figure 1. The body-frame of the car is attached at the rear contact point with

Fig. 1: LT-CAR model. The figure show the quantities used to describe the model.
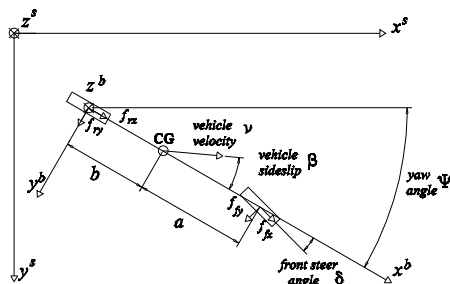
x-y-z axes oriented in a forward-right-down fashion. We let $\mathbf{x} = [x\ y\ z]^T \in \mathbb{R}^3$ and $R \in SO(3)$ denote the position

and orientation of the frame with respect to a fixed spatial-frame with x-y-z axes oriented in a north-east-down fashion. R maps vectors in the body frame to vectors in the spatial frame so that, for instance, the spatial angular velocity ω^s and the body angular velocity ω^b are related by $\omega^s = R\omega^b$ and $\omega^b = R^T\omega^s$. Similarly, $\mathbf{x}^s = \mathbf{x} + R\mathbf{x}^b$ gives the spatial coordinates of a point on the body with body coordinates $\mathbf{x}^b \in \mathbb{R}^3$. The orientation R of the (unconstrained) rigid car model can be parameterized (using Roll-Pitch-Yaw parametrization) as follows

$$
R = R(\psi, \theta) = R_z(\psi)R_y(\theta) = \begin{bmatrix} c_\psi c_\theta & -s_\psi & c_\psi s_\theta \\ s_\psi c_\theta & c_\psi & s_\psi s_\theta \\ -s_\theta & 0 & c_\theta \end{bmatrix},
$$

where θ and ψ are respectively the pitch and yaw angles (we use the notation $c_\psi = \cos(\psi)$, etc.). In the rest of the paper, for brevity, we use the notation $\phi = (\psi, \theta)$. The vector

$$
q = (x, y, \psi, z, \theta)^T = (q_r, q_c)^T
$$

provides a valid set of generalized coordinates for dynamics calculations. The coordinates $q_r = (x, y, \psi)^T$ are the *reduced* unconstrained car coordinates, while $q_c = (z, \theta)^T$ are the *constrained* coordinates.

A. Tire models

We model the tire forces by using a suitable version of the Pacejka's Magic Formula [26], [27]. Before, we clarify our notation. We use a subscript "f" ("r") for quantities of the front (rear) tire. When we want to give a generic expression that holds both for the front and the rear tire we just suppress the subscript. Thus, for example, we denote the generic normal tire force f_z, meaning that we are referring to f_{fz} for the front tire and f_{rz} for the rear one.

The rear and front forces tangent to the road plane, f_x and f_y, depend on the normal force and on the longitudinal and lateral slips. The longitudinal slip κ is the normalized difference between the angular velocity of the driven wheel ω_w and the angular velocity of the free-rolling $\omega_0 = v_{cx}/r_w$, with v_{cx} the contact point longitudinal velocity,

$$
\kappa = \frac{\omega_w - \omega_0}{\omega_0} = -\frac{v_{cx} - r_w\omega_w}{v_{cx}}.
$$

The lateral slip (or side-slip) β is defined as $\tan\beta = v_{cy}/v_{cx}$, with v_{cy} the lateral velocity. We assume that the rear and front forces tangent to the road plane, f_x and f_y, depend linearly on the normal forces. Thus, the combined slip forces are

$$
f_x = -f_z f_{x0}(\kappa)g_{x\beta}(k, \beta) = -f_z\mu_x(\kappa, \beta)
$$

$$
f_y = -f_z f_{y0}(\beta)g_{yk}(k, \beta) = -f_z\mu_y(\kappa, \beta),
$$

where the pure longitudinal slip $f_{x0}(\kappa)$, the pure lateral slip $f_{y0}(\beta)$ and the loss functions for combined slip $g_{x\beta}(\kappa, \beta)$ and $g_{yk}(\kappa, \beta)$ are defined in Appendix A together with the values of the parameters used in the paper.

The front forces expressed in the body frame, f_{fx}^b and f_{fy}^b, are obtained by rotating the forces in the tire frame according to the steering angle δ, so that, e.g., $f_{fx}^b = f_{fx}c_\delta - f_{fy}s_\delta$. Substituting the above expressions for f_{fx}

and f_{fy}, we get

$$f_{fx}^b = -f_{fz}\big(\mu_{fx}(\kappa_f, \beta_f)c_\delta - \mu_{fy}(\kappa_f, \beta_f)s_\delta\big)$$

$$:= -f_{fz}\tilde{\mu}_{fx}(\kappa_f, \beta_f, \delta).$$

In the rest of the paper, abusing notation, we will suppress the 'tilde' and use $\mu_{fx}(\kappa_f, \beta_f, \delta)$ to denote $\tilde{\mu}_{fx}(\kappa_f, \beta_f, \delta)$.

We assume to control either the rear slip κ_r and set $\kappa_f = 0$ (rear-wheel drive) or the front slip κ_f with $\kappa_r = 0$ (front-wheel drive). We denote κ the controlled slip. Thus, the *control inputs* of the car turn to be:

- κ, the rear or front longitudinal slip,
- δ, the front wheel steering angle.

Remark 2.1 (Longitudinal slip as control input): The use of the longitudinal slip as control input is present in the literature, e.g., [19] and [20]. This choice does not limit the applicability of our analysis. Indeed, wheel torques can be easily computed once a trajectory is computed. □

Next, we introduce a simplified tire model that will be used to design approximate trajectories (trajectories of a simplified car model) characterized by contact forces that can not be generated by the Pacejka's model. This simplified tire model, [4], [23], [28], relies on the following assumptions: (i) the longitudinal force is directly controlled, (ii) the relationship between the lateral force f_y and the side slip β is linear, and (iii) the longitudinal and lateral forces, f_x and f_y, are decoupled. We call the simplified car model obtained by using this tire approximation the Linear Tire LT-CAR (LT^2-CAR).

Figure 2 shows the plots of the longitudinal and lateral forces f_x and f_y for the Pacejka's and linear tire models.
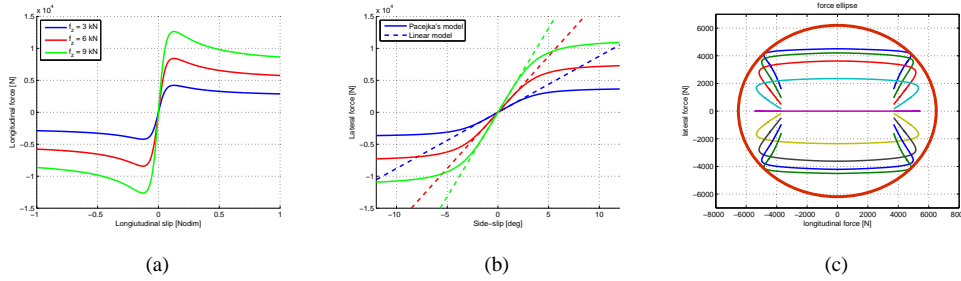

(a)   (b)   (c)

Fig. 2: Pure longitudinal (a) and lateral (b) forces are plotted as function of respectively longitudinal and lateral slip for three values of the normal force. In (b) the simplified tire model (dashed line) is also shown. The longitudinal versus lateral force is plotted as function of the longitudinal slip for different values of the side-slip (c). The ellipse of maximum tire forces is shown in solid red.

Remark 2.2 (Other tire models): Tires are one of the key components of the vehicle and have an important impact on the performance. To capture the complex behavior of the tires several models have been developed in the literature [26], [29], [30]. We highlight that the LT-CAR model can be developed with any tire model (not necessarily the Pacejka's one). □

B. Constrained Lagrangian dynamics

Next, we develop the constrained planar model of the rigid car that allows to include the load transfer. To describe the motion in the plane, we derive the equations of motion of the unconstrained system and explicitly incorporate the constraints (rather than choosing a subset of generalized coordinates). This allows to have an explicit expression for the normal (constraint) forces.

We derive the dynamics of the unconstrained system via the Euler-Lagrange equations. To do this, we define the Lagrangian $\mathcal{L}$ as the difference between the kinetic and potential energies $\mathcal{L}(q, \dot{q}) = T(q, \dot{q}) - V(q)$. The equations of motion for the unconstrained system are given by the Euler-Lagrange equations

$$\frac{d}{dt}\frac{\partial \mathcal{L}}{\partial \dot{q}}^T - \frac{\partial \mathcal{L}}{\partial q}^T = U \tag{1}$$

where U is the set of generalized forces. Exploiting the Euler-Lagrange equations, we get

$$M(q)\ddot{q} + C(q, \dot{q}) + G(q) = U \tag{2}$$

where $M(q)$, $C(q, \dot{q})$ and $G(q)$ are respectively the mass matrix, the Coriolis vector and the gravity vector.

The longitudinal and lateral forces arising from the tire-road interactions at the front and rear contact points, $f = [f_{fx}, f_{fy}, f_{rx}, f_{ry}]^T$, are converted into the generalized forces U by using the *principle of virtual work*, $<f, v_{cp}^b> = <U, \dot{q}>$, where $v_{cp}^b = [v_{fx}^b, v_{fy}^b, v_{rx}^b, v_{ry}^b]^T$ are the longitudinal and lateral velocities at the front and rear contact points. Computing the Jacobian matrix $J_f(\phi)$ mapping $\dot{q}$ to the front and rear contact point velocities expressed in the body frame, $v_{cp}^b = J_f(\phi)\dot{q}$, we get $< J_f(\phi)^T f, \dot{q} > = < U, \dot{q} >$, so that

$$U = J_f^T(\phi)f.$$

The front and rear contact points coordinates expressed in the body frame are $\mathbf{x}_f^b = (a + b, 0, 0)^T$ and $\mathbf{x}_r^b = (0, 0, 0)^T$. The coordinates in the spatial frame, respectively $\mathbf{x}_r^s = (x_r^s, y_r^s, z_r^s)$ and $\mathbf{x}_f^s = (x_f^s, y_f^s, z_f^s)$, are $\mathbf{x}_r^s = \mathbf{x}$ and $\mathbf{x}_f^s = \mathbf{x} + R\mathbf{x}_f^b$, so that the velocities in the spatial frame are given by $v_r^s = \dot{\mathbf{x}}$ and

$$v_f^s = \dot{\mathbf{x}} + R\,\omega^b \times \mathbf{x}_f^b = \dot{\mathbf{x}} - R\mathbf{x}_f^b \times \omega^b = \dot{\mathbf{x}} - R\hat{\mathbf{x}}_f^b J_{\omega^b}(\phi)\dot{\phi},$$

while the velocities expressed in the body frame are

$$v_r^b = R^T\dot{\mathbf{x}} = J_{v_r^b}(\phi)\dot{q}\,,$$

$$v_f^b = R^T\dot{\mathbf{x}} - \hat{\mathbf{x}}_f^b J_{\omega^b}(\phi)\dot{\phi} = J_{v_f^b}(\phi)\dot{q}\,.$$

Thus, the Jacobian J_f turns to be

$$J_f(\phi) = \begin{bmatrix} J_{v_{fx}^b} \\ J_{v_{fy}^b} \\ J_{v_{rx}^b} \\ J_{v_{ry}^b} \end{bmatrix} = \begin{bmatrix} c_\psi c_\theta & s_\psi c_\theta & 0 & -s_\theta & 0 \\ -s_\psi & c_\psi & (a+b)c_\theta & 0 & 0 \\ c_\psi c_\theta & s_\psi c_\theta & 0 & -s_\theta & 0 \\ -s_\psi & c_\psi & 0 & 0 & 0 \end{bmatrix}.$$

Next, we constrain the contact points to the road plane in order to compute the normal tire forces as reaction forces. We impose the constraint that the rear and front contact points have zero velocity along the z axis. The

velocity constraints are given by $\dot{z}_r = e_3^T R^T \dot{\mathbf{x}} = J_{v_{rz}^b}(\phi)\dot{q} = 0$, and $\dot{z}_f = e_3^T (R^T \dot{\mathbf{x}} - \hat{\mathbf{x}}_f^b J_{\omega^b}(\phi)\dot{\phi}) = J_{v_{fz}^b}(\phi)\dot{q} = 0$,

where z_r and z_f are the position of the rear and front contact point expressed in the body frame, respectively. The

front and rear constraints may be written in the form $A(q)\dot{q} = 0$, where

$$A(q) = \begin{bmatrix} J_{v_{fz}^b}(\phi) \\ J_{v_{rz}^b}(\phi) \end{bmatrix} = \begin{bmatrix} c_\psi s_\theta & s_\psi s_\theta & 0 & c_\theta & -(a+b) \\ c_\psi s_\theta & s_\psi s_\theta & 0 & c_\theta & 0 \end{bmatrix}. \tag{3}$$

From the principle of virtual work, we get the vector of constraint generalized forces, U_c, in terms of the contact

points constraint forces, $\lambda = [f_{fz}\ f_{rz}]^T \in \mathbb{R}^2$, as $U_c = A^T(q)\lambda$. These forces will be incorporated into the equations

of motion allowing the explicit calculation of the front and rear contact point forces, f_{fz} and f_{rz}.

In the next theorem we show that, under the linear dependence of the contact point forces on the normal ones,

the constrained system can be explicitly written as an unconstrained ordinary differential equation.

Theorem 2.3 (Special structure of the constrained system): Given the unconstrained car model with structure as

in (2) and the constraints (3), the following holds true:

(i) the dynamics of the constrained system can be written in terms of the unconstrained coordinates $q_r = [x, y, \psi]^T$

and the normal forces $\lambda = [f_{fz}\ f_{rz}]^T \in \mathbb{R}^2$ as

$$\tilde{\mathcal{M}}(q_r) \begin{bmatrix} \ddot{q}_r \\ \lambda \end{bmatrix} + \mathcal{C}(q_r, \dot{q}_r) + \mathcal{G}(q_r) = \mathcal{U}, \tag{4}$$

where

$$\tilde{\mathcal{M}}(q_r) = \begin{bmatrix} \mathcal{M}_{11}(q_r) & 0 \\ \mathcal{M}_{21}(q_r) & \mathcal{M}_{22}(q_r) \end{bmatrix} =$$

$$= \left[\begin{array}{ccc|cc} m & 0 & -mbs_\psi & 0 & 0 \\ 0 & m & mbc_\psi & 0 & 0 \\ -mbs_\psi & mbc_\psi & I_{zz} + mb^2 & 0 & 0 \\ \hline 0 & 0 & 0 & -1 & -1 \\ -mhc_\psi & -mhs_\psi & 0 & a+b & 0 \end{array} \right],$$

$$\mathcal{C}(q_r, \dot{q}_r) = \begin{bmatrix} \mathcal{C}_1(q_r, \dot{q}_r) \\ \mathcal{C}_2(q_r, \dot{q}_r) \end{bmatrix} = \left[\begin{array}{c} -mbc_\psi \dot{\psi}^2 \\ -mbs_\psi \dot{\psi}^2 \\ 0 \\ \hline 0 \\ (I_{xz} + mhb)\dot{\psi}^2 \end{array} \right], \tag{5}$$

$$\mathcal{G}(q_r) = \begin{bmatrix} \mathcal{G}_1(q_r) \\ \mathcal{G}_2(q_r) \end{bmatrix} = \left[\begin{array}{c} 0 \\ 0 \\ 0 \\ \hline -mg \\ mgb \end{array} \right], \tag{6}$$

$$\mathcal{U} = \left[\frac{\mathcal{U}_1}{0} \right] = \left[\begin{array}{cccc} c_\psi & -s_\psi & c_\psi & -s_\psi \\ s_\psi & c_\psi & s_\psi & c_\psi \\ 0 & a+b & 0 & 0 \\ \hline 0 & 0 & 0 & 0 \\ 0 & 0 & 0 & 0 \end{array} \right] \left[\begin{array}{c} f_{fx} \\ f_{fy} \\ f_{rx} \\ f_{ry} \end{array} \right]; \tag{7}$$

(ii) the subsystem

$$\mathcal{M}_{11}(q_r)\ddot{q}_r + \mathcal{C}_1(q_r, \dot{q}_r) + \mathcal{G}_1(q_r) = \mathcal{U}_1 \tag{8}$$

is a Lagrangian system obtained from a suitable *reduced Lagrangian* $\mathcal{L}_r(q_r)$, with constraint forces

$$\mathcal{M}_{21}(q_r)\ddot{q}_r + \mathcal{M}_{22}(q_r)\lambda + \mathcal{C}_2(q_r, \dot{q}_r) + \mathcal{G}_2(q_r) = 0;$$

(iii) under the assumption that the forces f depend linearly on the normal forces, i.e. $f = F\lambda$, the car dynamics turns to be

$$\mathcal{M}(q_r, \mu_{**}) \left[\begin{array}{c} \ddot{q}_r \\ \lambda \end{array} \right] + \mathcal{C}(q_r, \dot{q}_r) + \mathcal{G}(q_r) = 0 \tag{9}$$

with

$$\mathcal{M}(q_r, \mu_{**}) = \left[\begin{array}{cc} \mathcal{M}_{11}(q_r) & \mathcal{M}_{12}(q_r, \mu_{**}) \\ \mathcal{M}_{21}(q_r) & \mathcal{M}_{22}(q_r) \end{array} \right].$$

Proof: To prove statement (i), we use Lagrange's equations (1) including all the coordinates (even the constrained ones) and plug the constraints directly into the equations of motion (rather than attempting to eliminate the constraints by an appropriate choice of coordinates). The constraints are taken into account by adding the constraint forces into the equation of motion as additional forces which affect the motion of the system. Hence the constrained equations of motion can be written as

$$M(q)\ddot{q} + C(q, \dot{q}) + G(q) = J_f^T(q)f - A^T(q)\lambda$$

$$A(q)\ddot{q} + \dot{A}(q)\dot{q} = 0,$$

where M, C, G and A are the one introduced in (2) and (3). The constraints lead to $q_c(t) = \dot{q}_c(t) = \ddot{q}_c(t) = 0$, $\forall t \in \mathbb{R}$, so that we have

$$[M(q)\ddot{q} + C(q, \dot{q}) + G(q)]|_{q_c=0} = [J_f^T(q)f - A^T(q)\lambda]|_{q_c=0}$$

where

$$M(q)|_{q_c=0} = \left[\begin{array}{c|c} M_1(q_r) & M_2(q_r) \end{array} \right] =$$

$$= \left[\begin{array}{ccc|cc} m & 0 & -mbs_\psi & 0 & -mhc_\psi \\ 0 & m & mbc_\psi & 0 & -mhs_\psi \\ -mbs_\psi & mbc_\psi & mb^2 + I_{zz} & 0 & 0 \\ 0 & 0 & 0 & m & mb \\ -mhc_\psi & -mhs_\psi & 0 & mb & I_{yy} + m(b^2 + h^2) \end{array} \right]$$

$$A^T(q)|_{q_c=0} = \begin{bmatrix} 0 & 0 \\ 0 & 0 \\ 0 & 0 \\ 1 & 1 \\ -(a+b) & 0 \end{bmatrix},$$

and $C(q,\dot{q})|_{q_c=0}$, $G(q)|_{q_c=0}$, $J_f^T(q)f|_{q_c=0}$ are given by (5), (6), and (7) respectively. We rewrite the equations of motion with respect to the *extended variables* $[q_r, \lambda]^T$ as

$$[M_1(q_r)|A^T] \begin{bmatrix} \ddot{q}_r \\ \lambda \end{bmatrix} + \mathcal{C}(q_r, \dot{q}_r) + \mathcal{G}(q_r) = \begin{bmatrix} \mathcal{U}_1 \\ 0 \end{bmatrix}. \tag{10}$$

Defining $\tilde{\mathcal{M}} = [M_1(q_r)|A^T]$, the special structure (4) follows.

To prove statement (ii), we compute the reduced Lagrangian $\mathcal{L}_r(q_r) = T(q_r, \dot{q}_r) - V(q_r)$ and derive the Euler-Lagrange equations. Explicit calculations, shown in Appendix B, lead to equation (8). The expression of the constraint forces follows from the arguments to prove statement (i).

Finally, to prove (iii), if the forces f depend linearly on the reaction forces we have $f = F\lambda$, for a suitable F, then we can rewrite the generalized forces as

$$\begin{bmatrix} \mathcal{U}_1 \\ \hline 0 \end{bmatrix} = J_f^T(q_r)|_{q_c=0} \begin{bmatrix} -\mu_{fx} & 0 \\ -\mu_{fy} & 0 \\ 0 & -\mu_{rx} \\ 0 & -\mu_{ry} \end{bmatrix} \lambda$$

$$= - \begin{bmatrix} c_\psi\mu_{fx} - s_\psi\mu_{fy} & c_\psi\mu_{rx} - s_\psi\mu_{ry} \\ s_\psi\mu_{fx} + c_\psi\mu_{fy} & s_\psi\mu_{rx} + c_\psi\mu_{ry} \\ (a+b)\mu_{fy} & 0 \\ \hline 0 & 0 \\ 0 & 0 \end{bmatrix} \lambda := - \begin{bmatrix} \mathcal{M}_{12} \\ \hline 0 \end{bmatrix} \lambda,$$

so that equation (10) becomes

$$\tilde{\mathcal{M}}(q_r) \begin{bmatrix} \ddot{q}_r \\ \lambda \end{bmatrix} + \begin{bmatrix} 0 & \mathcal{M}_{12}(q_r, \mu_{**}) \\ \hline 0 & 0 \end{bmatrix} \begin{bmatrix} \ddot{q}_r \\ \lambda \end{bmatrix} + \mathcal{C} + \mathcal{G} = 0$$

from which equation (9) follows directly. ∎

We call the matrix $\mathcal{M}$ in (9) the *extended mass matrix*.

Remark 2.4: Equation (9) can be exploited as

$$\ddot{q}_r = -(\mathcal{M}_{11} + \mathcal{M}_{12}\mathcal{M}_{22}^{-1}\mathcal{M}_{21})^{-1}$$

$$[\mathcal{C}_1 + \mathcal{G}_1 + \mathcal{M}_{12}\mathcal{M}_{22}^{-1}(\mathcal{C}_2 + \mathcal{G}_2)]$$

$$\lambda = -\mathcal{M}_{22}^{-1}(\mathcal{C}_2 + \mathcal{G}_2 + \mathcal{M}_{21}\ddot{q}_r).$$

From this expression it is clear that we have a dynamic model explicitly depending on the unconstrained coordinates x, y and ψ and an explicit expression for the normal forces that can be used to calculate the Pacejka's term for the tire forces. □

An important aspect to investigate for the constrained model is the invertibility of the extended mass matrix. Differently from the standard mass matrix, which is always positive definite (and thus invertible), the invertibility of the extended mass matrix depends on the model and tire parameters.

Theorem 2.5 (Invertibility of the extended mass matrix): The extended mass matrix $\mathcal{M}$ is invertible if and only if

$$(\mu_{rx} - \mu_{fx}) \neq \frac{a+b}{h}.$$

Proof: Clearly, a matrix is invertible (i.e. non-singular) if and only if its determinant is nonzero. By performing elementary row operations on the $\mathcal{M}$ matrix (Gauss-Jordan elimination method), we get the equivalent matrix

$$\left[\begin{array}{cc|ccc} m & 0 & -mbs_\psi & c_\psi\mu_{fx} - s_\psi\mu_{fy} & c_\psi\mu_{rx} - s_\psi\mu_{ry} \\ 0 & m & mbc_\psi & s_\psi\mu_{fx} + c_\psi\mu_{fy} & s_\psi\mu_{rx} + c_\psi\mu_{ry} \\ \hline 0 & 0 & I_{zz} & a\mu_{fy} & -b\mu_{ry} \\ 0 & 0 & 0 & -1 & -1 \\ 0 & 0 & 0 & a+b+h\mu_{fx} & h\mu_{rx} \end{array}\right].$$

With the matrix in this new form, the determinant can be easily computed and is given by $\det\mathcal{M} = m^2 I_{zz}(-\mu_{rx}h + a + b + \mu_{fx}h)$, which is zero if and only if $(\mu_{rx} - \mu_{fx}) = \frac{a+b}{h}$, thus concluding the proof. ∎

Corollary 2.6: For the car parameters and Pacejka's tire model in Appendix A, the extended mass matrix is invertible.

Proof: From the combined slip Pacejka's formulas we can show that μ_{rx} and μ_{fx} are bounded,

$$|\mu_{rx}| = |f_{rx0}(\kappa)g_{rx\beta}(\kappa,\beta_r)| \leq d_x^r$$

$$|\mu_{fx}| = |c_\delta f_{fx0}(0)g_{fx\beta}(\beta) - s_\delta f_{fy0}(\beta)g_{fx\beta}(\beta)|$$

$$\leq (d_x^f + d_y^f).$$

Thus, $|\mu_{rx} - \mu_{fx}| \leq (d_x^r + d_x^f + d_y^f)$ and for the data provided in Appendix A, we have the strict inequality $(d_x^r + d_x^f + d_y^f) < \frac{a+b}{h}$, so that the proof follows. ∎

C. Dynamics in the body frame

We provide the dynamics in the body frame with two different set of coordinates. These dynamics will be helpful in the characterization of the equilibrium manifold and in the exploration strategy. Indeed, expressing the dynamics in the body frame, we can decouple the dynamic of the vehicle from its kinematics. This allows to write a reduced model that includes only velocities and accelerations.

Since the dynamics do not depend on the positions x and y, and the orientation ψ, we can work directly with the longitudinal velocity v_x and the lateral velocity v_y. To do this, note that

$$\begin{bmatrix} \ddot{x} \\ \ddot{y} \end{bmatrix} = R_z(\psi) \begin{bmatrix} \dot{v}_x - v_y\dot{\psi} \\ \dot{v}_y + v_x\dot{\psi} \end{bmatrix}. \tag{11}$$

Thus, we get the equations in (12).

$$
\begin{bmatrix} m & 0 & 0 & \mu_{fx} & \mu_{rx} \\ 0 & m & mb & \mu_{fy} & \mu_{ry} \\ 0 & mb & (I_{zz}+mb^2) & (a+b)\mu_{fy} & 0 \\ 0 & 0 & 0 & -1 & -1 \\ -mh & 0 & 0 & a+b & 0 \end{bmatrix} \begin{bmatrix} \dot{v}_x \\ \dot{v}_y \\ \ddot{\psi} \\ f_{fz} \\ f_{rz} \end{bmatrix} + \begin{bmatrix} -mb\dot{\psi}^2 - mv_y\dot{\psi} \\ mv_x\dot{\psi} \\ mbv_x\dot{\psi} \\ 0 \\ (I_{xz}+mhb)\dot{\psi}^2 + mhv_y\dot{\psi} \end{bmatrix} + \begin{bmatrix} 0 \\ 0 \\ 0 \\ -mg \\ mgb \end{bmatrix} = \begin{bmatrix} 0 \\ 0 \\ 0 \\ 0 \\ 0 \end{bmatrix} \tag{12}
$$

$$
\begin{bmatrix} mc_\beta & -mvs_\beta & 0 & \mu_{fx} & \mu_{rx} \\ ms_\beta & mvc_\beta & mb & \mu_{fy} & \mu_{ry} \\ mbs_\beta & mbvc_\beta & (I_{zz}+mb^2) & (a+b)\mu_{fy} & 0 \\ 0 & 0 & 0 & -1 & -1 \\ -mhc_\beta & mhvs_\beta & 0 & a+b & 0 \end{bmatrix} \begin{bmatrix} \dot{v} \\ \dot{\beta} \\ \ddot{\psi} \\ f_{fz} \\ f_{rz} \end{bmatrix} + \begin{bmatrix} -mv\dot{\psi}s_\beta - mb\dot{\psi}^2 \\ -mv\dot{\psi}c_\beta \\ mbv\dot{\psi}c_\beta \\ 0 \\ (I_{xz}+mhb)\dot{\psi}^2 + mhv\dot{\psi}s_\beta \end{bmatrix} + \begin{bmatrix} 0 \\ 0 \\ 0 \\ -mg \\ mgb \end{bmatrix} = \begin{bmatrix} 0 \\ 0 \\ 0 \\ 0 \\ 0 \end{bmatrix}
$$
$$\tag{13}$$

One more version of the dynamics is obtained by choosing as states the vehicle speed v and the vehicle side-slip angle β, where $\tan\beta = v_y/v_x$. This change of coordinates is helpful to calculate the equilibrium manifold in the next section. In this case, denoting $\chi = \psi + \beta$ the orientation of the velocity with respect to the spatial frame, we have

$$
\begin{bmatrix} \ddot{x} \\ \ddot{y} \end{bmatrix} = R_z(\chi) \begin{bmatrix} \dot{v} \\ v\dot{\chi} \end{bmatrix} = R_z(\psi)R_z(\beta) \begin{bmatrix} \dot{v} \\ v\dot{\chi} \end{bmatrix},
$$

where $\dot{v}$ and $v\dot{\chi}$ are the longitudinal and lateral accelerations, respectively. Finally, considering the relation (11) we have

$$
\begin{bmatrix} \dot{v} \\ v\dot{\beta} \end{bmatrix} = R_z(\beta)^T \begin{bmatrix} \dot{v}_x - v_y\dot{\psi} \\ \dot{v}_y + v_x\dot{\psi} \end{bmatrix} - \begin{bmatrix} 0 \\ v\dot{\psi} \end{bmatrix},
$$

and the equations of motion are given in (13).

We have a family of car models, (12) and (13), that provide different insights depending on the features to investigate. The model (12) is used to explore the dynamics of the car vehicle; the models (12) and (13) are used to solve the equilibrium manifold (under usual driving conditions, it is natural to specify v and β).

III. EQUILIBRIUM MANIFOLD

In this section we analyze the equilibrium manifold of the car model, i.e. the set of trajectories that can be performed by use of constant inputs. Searching for "constant" trajectories requires the solution of a set of nonlinear equations expressing the fact that all accelerations must be set to zero. To define an equilibrium trajectory, we refer to the car model in the form (13). The equilibria are obtained by enforcing

$$
(\dot{v}, \dot{\beta}, \ddot{\psi}) = (0, 0, 0). \tag{14}
$$

The corresponding trajectory of the full car model (including position and orientation) is a circular path at constant speed v, yaw rate $\dot{\psi}$ and vehicle side-slip angle β. Since $\dot{\beta} = 0$, the lateral acceleration is given by $a_{lat} = v\dot{\psi}$, and

expressing the accelerations in the body frame as follows,

$$\begin{bmatrix} a_x \\ a_y \end{bmatrix} = \begin{bmatrix} \dot{v}_x - v_y \dot{\psi} \\ \dot{v}_y + v_x \dot{\psi} \end{bmatrix} = R_z(\beta) \begin{bmatrix} \dot{v} \\ v\dot{\chi} \end{bmatrix}$$

we have

$$a_x = -a_{lat} \sin \beta$$

$$a_y = a_{lat} \cos \beta$$

$$\dot{\psi} = a_{lat}/v.$$

Now, referring to the dynamic model (13), we set the constraints (14) and we get two equations from the load transfer in equilibrium condition

$$-f_{fz} = mg\frac{b}{a+b} + \frac{(I_{xz} + mhb)(\frac{a_{lat}}{v})^2 + a_{lat}mh\sin\beta}{a+b}$$

$$-f_{rz} = mg\frac{a}{a+b} - \frac{(I_{xz} + mhb)(\frac{a_{lat}}{v})^2 + a_{lat}mh\sin\beta}{a+b}$$

and the following three equations from the system dynamics:

$$ma_x - mb\dot{\psi}^2 + \mu_{fx}f_{fz} + \mu_{rx}f_{rz} = 0$$

$$ma_y + \mu_{fy}f_{fz} + \mu_{ry}f_{rz} = 0 \qquad (15)$$

$$mba_y + (a+b)\mu_{fy}f_{fz} = 0.$$

Substituting the expression of the normal forces f_{fz} and f_{rz} into equations (15), we obtain a nonlinear system of three equations in five unknowns (v, a_{lat}, β, δ and κ), so that the equilibrium manifold is a two-dimensional surface.

We parameterize the equilibrium manifold in terms of the car speed and lateral acceleration (v and a_{lat}), so that the slip angle, steering angle and longitudinal slip (β, δ and κ) are obtained by solving the nonlinear equations in (15).

We solve the nonlinear system by using a Predictor-Corrector (PC) continuation method, [22], relying on the continuity of the equilibria with respect to the equilibrium manifold parameters v and a_{lat}.

Next, we describe the PC continuation method applied to the equilibrium manifold of our car model. We fix the velocity v and explore a one-dimensional slice of the manifold.

First, we provide a useful lemma from [22].

Lemma 3.1 (Lemma 2.1.3, [22]): Let $\ell : \mathbb{R}^{n+1} \to \mathbb{R}^n$ be a smooth nonlinear function such that $\ell(\eta_0) = 0$ for some $\eta_0 \in \mathbb{R}^{n+1}$ and let the *Jacobian matrix* $D_\ell(\eta_0) \in \mathbb{R}^{n \times (n+1)}$ have maximum rank. Then, there exists a smooth curve $s \in [0, s_1) \mapsto c(s) \in \mathbb{R}^{n+1}$, parametrized with respect to arclength s, for some open interval $[0, s_1)$ such that for all $s \in [0, s_1)$:

- $c(0) = \eta_0$;
- $\ell(c(s)) = 0$;
- $rank(D_\ell(c(s))) = n$;

- $\dot{c}(s) \neq 0$. □

Let $\eta = (a_{lat}, \beta, \delta, \kappa)^T$ and let $\ell(\eta) = 0$ be the nonlinear system in (15), with $\ell : \mathbb{R}^4 \to \mathbb{R}^3$. The following proposition shows that there exists a one dimensional manifold of solution points.

Proposition 3.2 (Equilibrium manifold well posedness): Given the nonlinear system in (15), the following holds true:

(i) there exists a smooth curve $s \in [0, s_1) \mapsto c(s) \in \mathbb{R}^4$, for some $s_1 > 0$, such that $\ell(c(s)) = 0$ for all $s \in [0, s_1)$;

(ii) $c(s)$ is the local solution of

$$\dot{\eta} = t(D_\ell(\eta))$$

$$\eta(0) = \eta_0,$$

(16)

where $t(D_\ell(\eta))$ is the *tangent vector induced by* $D_\ell(\eta)$.

Proof: To prove statement (i), we use Lemma 3.1. The nonlinear function ℓ contains sums and products of trigonometric and power functions, thus it is smooth. Using the expression of the combined slip forces introduced in Section II-A, for $\eta_0 = (0, 0, 0, 0)$ we have $\mu_{**} = 0$, so that it follows easily that $\ell(\eta_0) = 0$. Moreover, by explicit calculation, the Jacobian matrix at η_0 has rank three.

To prove statement (ii), we differentiate $\ell(c(s)) = 0$ with respect to the arc-length s. The tangent $\dot{c}(s)$ satisfies the equation $D_\ell(c(s))\dot{c}(s) = 0$, $\|\dot{c}(s)\| = 1 \ \forall s \in [0, s_1)$. Hence $\dot{c}(s)$ spans the one-dimensional kernel $ker(D_\ell(c(s)))$, or equivalently, $\dot{c}(s)$ is orthogonal to all rows of $D_\ell(c(s))$. In other words, the unique vector $\dot{c}(s)$ is the tangent vector induced by $D_\ell(c(s))$, $t(D_\ell(c(s)))$. Using the Implicit Function Theorem, e.g., [31], the tangent vector $t(D_\ell(c(s)))$ depends smoothly on $D_\ell(c(s))$. Thus, c is the solution curve of the initial value problem in (16), which concludes the proof. ∎

In order to numerically trace the curve c efficiently, we use a Predictor-Corrector (PC) method. The main idea is to generate a sequence of points along the curve η_i, $i = 1, 2, \ldots$, that satisfy a given tolerance, say $\|\ell(\eta_i)\| \leq \nu$ for some $\nu > 0$. So, for $\nu > 0$ sufficiently small, there is a unique parameter value s_i such that the point $c(s_i)$ on the curve is nearest to η_i in Euclidean norm. To describe how points η_i along the curve c are generated, suppose that a point $\eta_i \in \mathbb{R}^4$ satisfies the chosen tolerance (i.e. $\|\ell(\eta_i)\| \leq \nu$). If η_i is a regular point of ℓ, then there exists a unique solution curve $c_i : [0, s_1) \to \mathbb{R}^4$ which satisfies the initial value problem (16) with initial condition $\eta(0) = \eta_i$.

To obtain a new point η_{i+1} along c, we make a *predictor step* as a simple numerical integration step for the initial value problem. We use an *Euler predictor*:

$$\alpha_{i+1} = \eta_i + \epsilon \, t(D_\ell(\eta_i)),$$

where $\epsilon > 0$ represents a suitable stepsize.

The corrector step computes the point ω_{i+1} on c which is nearest to α_{i+1}. The point ω_{i+1} is found by solving the optimization problem

$$\|\omega_{i+1} - \alpha_{i+1}\| = \min_{\ell(\omega)=0} \|\omega - \alpha_{i+1}\|.$$

(17)

If the stepsize ϵ is sufficiently small (so that the predictor point α_{i+1} is sufficiently close to the curve c) the minimization problem has a unique solution ω_{i+1}. We compute ω_{i+1} by using a Newton-like method. The *Newton point $\mathcal{N}(\alpha)$* for approximating the solution of (17) is given by $\mathcal{N}(\alpha) = \alpha - D_\ell(\alpha)^\dagger \ell(\alpha)$.

The PC continuation method used in the paper thus consists of repeatedly performing these predictor and corrector steps as shown in the pseudo-code below.

Algorithm 1 PC-continuation method

Given: initial equilibrium condition η_0 such that $\ell(\eta_0) = 0$

  for $i = 0, 1, 2 \ldots$ **do**

    set the initial steplength $\epsilon_i = \overline{\epsilon}$;

    loop

      get predictor step: $\alpha_{i+1} = \eta_i + \epsilon_i\, t(D_\ell(\eta_i))$;

      search corrector term:

$$\omega_{i+1} = \alpha_{i+1} - D_\ell(\alpha_{i+1})^\dagger \ell(\alpha_{i+1});$$

$$\alpha_{i+1} = \omega_{i+1};$$

     if convergence **then**

      break;

     else

      update the steplength $\epsilon_{i+1} = \epsilon_i/2$;

     end if

    end loop

    $\eta_{i+1} = \omega_{i+1}$;

  end for

We compute and compare the equilibrium manifold for two car configurations, namely a saloon car with front-wheel drive ($\kappa = \kappa_f$) and a sports car with rear-wheel drive ($\kappa = \kappa_r$), equipped with the same set of tires. The parameters of the two cars and the tires are given in Appendix A.

Some slices of the equilibrium manifold are shown in Figure 3. For low longitudinal and lateral slips a first class of equilibria appears. These equilibria are close to the ones with the linear tire approximation (the solid lines in Figures 3a and 3b and Figures 3e and 3f are close to the dot lines). Indeed, for low slips ($\beta_r, \beta_f < 5[deg]$ and $\kappa < 0.005$) the tires work within their linear region as appears in Figures 2a and 2b. To characterize the vehicle behavior in this region, we can use, [5], the *understeer gradient*

$$K_{us}(a_{lat}; v) = \frac{\partial \delta(a_{lat}; v)}{\partial a_{lat}} - K_a,$$

where $K_a = \frac{a+b}{v^2}$ is called Ackerman steer angle gradient. The vehicle is said to be understeering if $K_{us} > 0$, neutral if $K_{us} = 0$ and oversteering if $K_{us} < 0$. From a graphical point of view, the understeering behavior can be
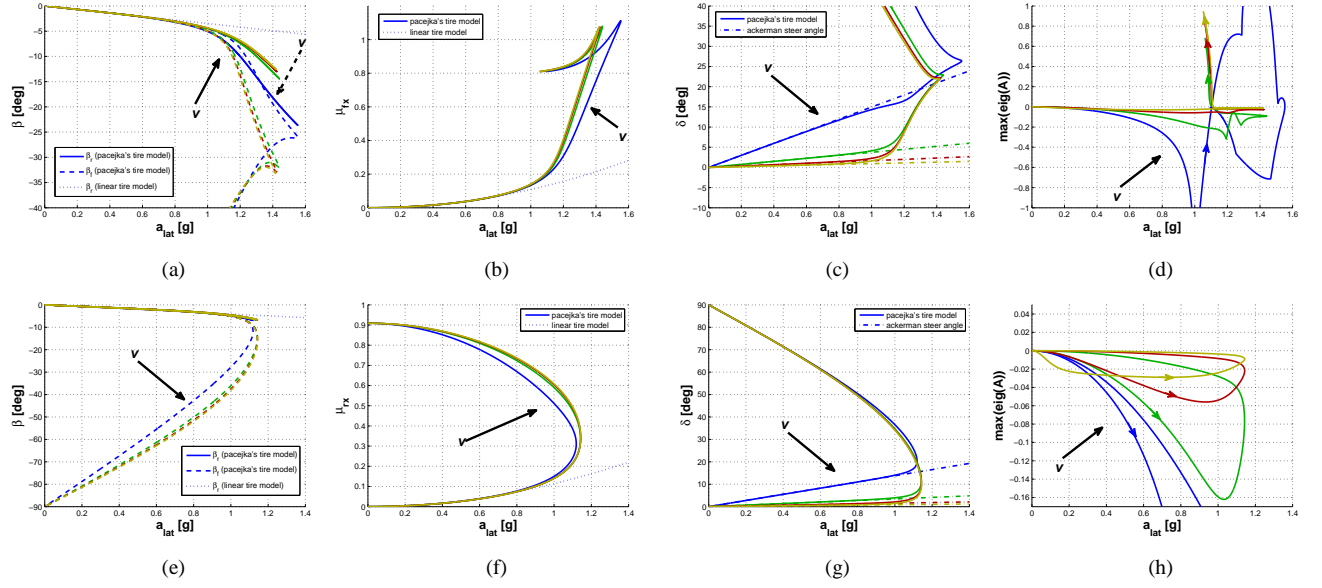
Fig. 3: Equilibrium manifold for the front-wheel drive saloon car (a)-(d) and for the rear-wheel drive sports car (e)-(h). Specifically: rear and front side slip, longitudinal force coefficient, steering angle, and maximum eigenvalue for $v = (10, 20, 30, 40)m/s$. Dash lines in (a)-(b) and (e)-(f) are the equilibria with linear tire model at $v = 20m/s$. The dash-dot line in (c) and (g) is the Ackerman steer angle.
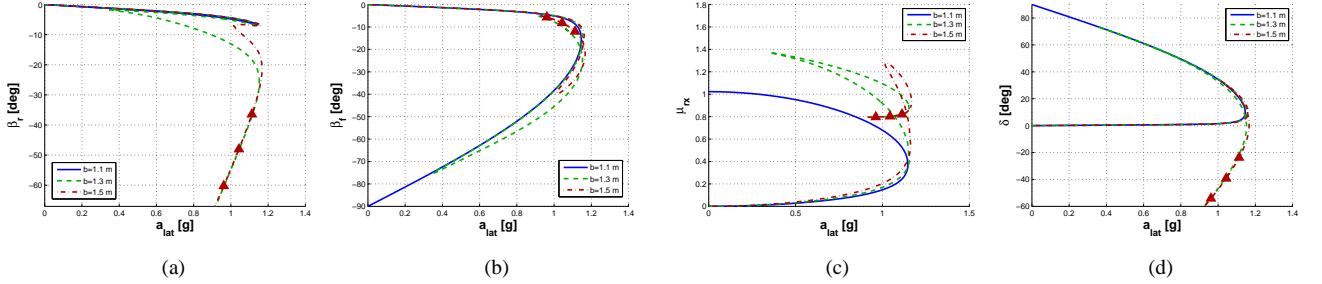

Fig. 4: Equilibrium manifold for the rear-wheel drive sports car for different positions of the center of mass. Specifically: rear side slip, front side slip, longitudinal force coefficient and steering angle for $v = 40m/s$, $b = (1.1, 1.3, 1.5)m$ and $a + b = 2.45m$. In (d) the red diamond markers show three equilibrium points with steering angle opposite to the direction of the turn (counter-steering).

measured by looking at how much the curve $a_{lat} \mapsto \delta(a_{lat}; v)$, for fixed v, departs from the line $a_{lat} \mapsto K_a a_{lat}$. As shown in Figure 3c, for the saloon car the steer angle gradient is slightly positive, which suggests an understeering behavior, except in the case of $v = 10[m/s]$ (slightly oversteering). For the sports car, Figure 3g, we observe a less understeering (nearly neutral) behavior $K_{us} \simeq 0$ at higher speeds.

For high values of the longitudinal and lateral slips the equilibrium manifolds depart from their linear-tire approximation. Indeed, the linear tires, without force saturation, allow to generate a lateral force for any lateral

acceleration. In this region we can not use the understeer gradient analysis, thus we study the stability of the equilibria. The stability is investigated by calculating the leading eigenvalues (those with largest real part) of the linearized system with respect to the equilibrium states. In this region the equilibria are unstable for the saloon car, see Figure 3d, and stable for the sports car, see Figure 3h.

The PC-continuation method allows also to perform a sensitivity analysis of the equilibrium manifold with respect to the car parameters (as, e.g., mass, moment of inertia, center of mass position). In Figure 4 we highlight the results obtained when varying the center of mass position along the body longitudinal axis. By setting the sports car inertial parameters, we compute the manifold varying the value of a and b with constant wheelbase $a + b = 2.45$m.

As far as the center of mass stays between the rear contact point and the half wheelbase, the equilibrium manifold (Figure 4 blue line) is structurally the same as the one in Figure 3e, 3f and 3g. When the center of mass is moved over the half wheelbase toward the front axle the manifold has a significantly different structure (green and red lines). In particular, the equilibria at highest rear lateral and longitudinal slips, highlighted with the red diamond markers, are achieved with steering angle opposite to the direction of the turn (counter-steering). This car set up resembles the one of rally cars which, indeed, take advantage of the counter-steering behavior in performing aggressive turns.

The significant change of the equilibrium manifold with respect to the position of the center of mass suggests that the equilibrium manifold sensitivity analysis can be used as a design tool to optimize the car performance.

IV. NONLINEAR OPTIMAL CONTROL BASED TRAJECTORY EXPLORATION

In this section we describe the optimal control based strategies used to explore the dynamics of the car vehicle and provide numerical computations showing their effectiveness.

A. Least-square optimization for trajectory exploration

Complex dynamic interactions make the development of maneuvers highly nontrivial. To this end, we use nonlinear least squares trajectory optimization to explore system trajectories. That is, we consider the optimal control problem

$$\min \ \frac{1}{2} \int_0^T \|\mathbf{x}(\tau) - \mathbf{x}_d(\tau)\|_Q^2 + \|\mathbf{u}(\tau) - \mathbf{u}_d(\tau)\|_R^2 d\tau$$
$$+ \frac{1}{2} \|\mathbf{x}(T) - \mathbf{x}_d(T)\|_{P_1}^2$$
$$\text{subj. to} \ \ \dot{\mathbf{x}}(t) = f(\mathbf{x}(t), \mathbf{u}(t)) \qquad \mathbf{x}(0) = \mathbf{x}_0,$$

where Q, R and P_1 are positive definite weighting matrices, for $z \in \mathbb{R}^n$ and $W \in \mathbb{R}^{n \times n}$ $\|z\|_W^2 = z^T W z$, and $(\mathbf{x}_d(\cdot), \mathbf{u}_d(\cdot))$ is a desired curve. The desired curve is a trajectory exploration design *parameter*, i.e., it is a naive guess of a system trajectory that the designer uses to explore the trajectory space. Here the weights Q, R, and P_1 are design variables that reflect the relative importance (and/or confidence) of certain components of the desired

trajectory. Writing the least squares trajectory functional as

$$h(\xi; \xi_d) = \frac{1}{2} \int_0^T \|\mathbf{x}(\tau) - \mathbf{x}_d(\tau)\|_Q^2 + \|\mathbf{u}(\tau) - \mathbf{u}_d(\tau)\|_R^2 \, d\tau$$
$$+ \frac{1}{2} \|\mathbf{x}(T) - \mathbf{x}_d(T)\|_{P_1}^2$$

with $\xi = (\mathbf{x}(\cdot), \mathbf{u}(\cdot))$ and $\xi_d = (\mathbf{x}_d(\cdot), \mathbf{u}_d(\cdot))$, and denoting $\mathcal{T}$ the manifold of bounded trajectories $(\mathbf{x}(\cdot), \mathbf{u}(\cdot))$ on $[0, T]$, the optimization problem can be written as

$$\min_{\xi \in \mathcal{T}} h(\xi; \xi_d). \tag{18}$$

To facilitate the local exploration of trajectories of this highly coupled nonlinear system, we use the Projection Operator Newton method developed in [24].

We take a trajectory tracking approach, defining a projection operator that maps a state-control curve (e.g., a desired curve) onto the trajectory manifold. Specifically, the time varying-trajectory tracking control law

$$\dot{\mathbf{x}}(t) = f(\mathbf{x}(t), \mathbf{u}(t)), \qquad \mathbf{x}(0) = \mathbf{x}_0,$$
$$\mathbf{u}(t) = \mu(t) + K(t)(\alpha(t) - \mathbf{x}(t)) \tag{19}$$

defines the projection operator

$$\mathcal{P} : \xi = (\alpha(\cdot), \mu(\cdot)) \mapsto \eta = (\mathbf{x}(\cdot), \mathbf{u}(\cdot)),$$

mapping the curve ξ to the trajectory η.

Using the projection operator to locally parametrize the trajectory manifold, we may convert the constrained optimization problem (18) into one of minimizing the unconstrained functional $g(\xi; \xi_d) = h(P(\xi); \xi_d)$ using, for example, a Newton descent method as described below. A geometric representation of the projection operator is shown in Figure 5.
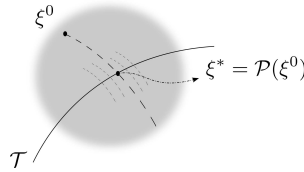

Fig. 5: Geometric representation of the trajectory manifold: every point of $\mathcal{T}$ is a trajectory of the system. The projection of the curve $\xi^0 = (\alpha(\cdot), \mu(\cdot))$ on $\mathcal{T}$ through $\mathcal{P}$ is the trajectory $\xi^* = (\mathbf{x}(\cdot), \mathbf{u}(\cdot))$.

Minimization of the trajectory functional is accomplished by iterating over the algorithm shown in the table, where ξ_i indicates the current trajectory iterate, ξ_0 an initial trajectory, and $\zeta \mapsto Dg(\xi_i; \xi_d) \cdot \zeta$ and $\zeta \mapsto D^2 g(\xi_i; \xi_d)(\zeta, \zeta)$ are respectively the first and second Fréchet differentials of the functional $g(\xi) = h(\mathcal{P}(\xi); \xi_d)$ at ξ_i.

Algorithm 2 Projection operator Newton method

Given: initial trajectory $\xi_0 \in \mathcal{T}$

  for $i = 0, 1, 2 \ldots$ **do**

    design K defining $\mathcal{P}$ about ξ_i

    search for descent direction

$$\zeta_i = \arg \min_{\zeta \in T_{\xi_i} \mathcal{T}} Dg(\xi_i; \xi_d) \cdot \zeta + \frac{1}{2} D^2 g(\xi_i; \xi_d)(\zeta, \zeta)$$

    step size $\gamma_i = \arg \min_{\gamma \in (0,1]} g(\xi + \gamma \zeta_i)$;

    project $\xi_{i+1} = \mathcal{P}(\xi_i + \gamma_i \zeta_i)$.

  end for

The algorithm has the structure of a standard Newton method for the minimization of an unconstrained function. The key points are the design of K defining the projection operator and the computation of the derivatives of g to "search for descent direction". It is worth noting that these two steps involve the solution of suitable (well known) linear quadratic optimal control problems, [24].

B. Exploration strategy

The projection operator Newton method, being a descent method, guarantees the convergence to a local minimum of the optimal control problem in (18). A naive choice of the desired curve and the initial trajectory may let the algorithm converge to a (local minimum) trajectory that is too far from the desired curve and does not contain useful information on the vehicle capabilities. In order to deal with this issue, we develop an exploration strategy based on the following features: (i) choose a desired curve that well describes the desired behavior of the vehicle, but is not "too far from the trajectory manifold", (ii) embed the optimal control problem into a class of problems parametrized by the desired trajectory, (iii) design a continuation strategy to update the desired and initial trajectories of the embedding problems.

First, we describe how to choose the desired curve. The path and the velocity profile to follow on that path, are usually driven by the exploration objective. Thus, the positions $x_d(t)$ and $y_d(t)$ and the velocity $v_d(t)$, with $t \in [0, T]$, of the desired curve are assigned. For example, in the next sections we describe two maneuvers where we want to understand the vehicle capabilities in following respectively a chicane at "maximum speed" and a real testing track at constant speed.

How to choose the other portion of the desired curve (i.e. the remaining states and the inputs) strongly affects the exploration process. In order to choose this portion of the desired curve, we use a quasi trajectory that, with some abuse of notation, we call *quasi-static trajectory*.

Given $x_d(t)$, $y_d(t)$ and $v_d(t)$ (and thus $\sigma_d(t)$), $t \in [0, T]$, for each $t \in [0, T]$, we impose the equilibrium conditions (14) for the desired velocity and path curvature at t. That is, posing $v_{qs}(t) = v_d(t)$ and $\dot{\psi}_{qs}(t) =$

$v_d(t)\sigma_d(t)$, we compute the corresponding equilibrium value for the sideslip angle, $\beta_{qs}(t)$, the yaw rate, $\dot{\psi}_{qs}(t)$, and the yaw angle, $\psi_{qs}(t)$, together with the steering angle, $\delta_{qs}(t)$, and the longitudinal slip, $\kappa_{qs}(t)$, by solving the nonlinear equations (15). Thus, the quasi-static trajectory $(\mathrm{x}_{qs}(t), \mathrm{u}_{qs}(t))$, $t \in [0, T]$, is given by

$$\mathrm{x}_{qs}(t) = [x_d(t), \, y_d(t), \, \psi_{qs}(t), \, v_d(t), \, \beta_{qs}(t), \, v_d(t)\sigma_d(t)]^T \, ,$$

$$\mathrm{u}_{qs}(t) = [\delta_{qs}(t), \, \kappa_{qs}(t)]^T \, .$$

Remark 4.1: We stress that the quasi-static trajectory is not an LT-CAR trajectory since it does not satisfy the dynamics. However, experience shows that, reasonably, for low values of the (longitudinal and lateral) accelerations, the quasi-static trajectory is close to the trajectory manifold. □

The above considerations suggest that the quasi-static trajectory represents a reasonable guess of the system trajectory on a desired track for a given velocity profile. Thus, when only the desired position and velocity curves are available, we set the desired curve as the quasi-static trajectory. In doing this choice we remember that the positions and velocity profiles are the ones we really want to track, whereas the other state profiles are just a guess. Thus, we will weight the first much more than the latter.

Since we are interested in exploring "limit" vehicle capabilities, most of the times, as it happens in real prototype tests, we will study aggressive (cornering) maneuvers that are usually characterized by high levels of lateral acceleration. Thus, it can happen that a quasi-static trajectory can not be found (we are out of the equilibrium manifold). If this is the case, we generate the desired curve by using the linear tires car model, LT^2-CAR, discussed in Section II-A, so that every lateral acceleration can be achieved. In this way we can always construct the quasi-static trajectory, and thus the desired curve, from a given desired path and velocity profile.

Remark 4.2: We could optimize on the simplified LT-CAR model, find an optimal trajectory of the simplified model and use that one as a desired trajectory for the actual LT-CAR model. However, we can leave the optimization do this operation directly on the actual model. □

With the desired curve in hand we still have the issue of choosing the initial trajectory to apply the projection operator Newton method. To design the initial trajectory, we could choose an equilibrium trajectory (e.g. a constant velocity on a straight line). However, such naive initial trajectory could lead to a local minimum that is significantly far from the desired behavior or cause a relatively high number of iterations. From the considerations in Remark 4.1, we know that a quasi-static trajectory obtained by a velocity profile that is not "too aggressive" is reasonably close to the trajectory manifold.

These observations motivate and inspire the development of an embedding and continuation strategy. We parametrize the optimal control problem in (18) with respect to the desired curve. Namely, we design a *family of desired curves* that continuously morph a quasi-static trajectory with a "non-aggressive" velocity profile into the actual desired (quasi-static) curve.

Thus, the continuation update is as follows. We start with a non-aggressive desired curve, $\xi_d^1 = (\mathrm{x}_d^1(\cdot), \mathrm{u}_d^1(\cdot))$, and choose as initial trajectory, ξ_0^1, the projection of the desired curve, $\xi_0^1 = \mathcal{P}(\xi_d^1)$. That is, we implement equation (19) with $(\alpha(\cdot), \mu(\cdot)) = (\mathrm{x}_d^1(\cdot), \mathrm{u}_d^1(\cdot))$. Then, we update the temporary desired curve, ξ_d^i, with the new curve in the

family, ξ_d^{i+1}, (characterized by a more aggressive velocity profile on the same track) and use as initial trajectory for the new problem the optimal trajectory at the previous step. The procedure ends when an optimal trajectory is computed for the optimal control problem where the temporary desired curve equals the actual one. Next, we give a pseudo code description of the exploration strategy. We denote PO_Newt(ξ_i, ξ_d) the local minimum trajectory obtained by implementing the projection operator Newton method for a given desired curve ξ_d and initial trajectory ξ_i.

Algorithm 3 Exploration strategy

Given: desired path and velocity $x_d(\cdot)$, $y_d(\cdot)$ and $v_d(\cdot)$

    compute: desired curve $\xi_d = (\mathrm{x}_{qs}(\cdot), \mathrm{u}_{qs}(\cdot))$;

    design: ξ_d^i, $i \in \{1, \ldots, n\}$,

            s.t. $\mathcal{P}(\xi_d^1) \simeq \xi_d^1$ and $\xi_d^n = \xi_d$;

    compute: initial trajectory $\xi_0^1 = \mathcal{P}(\xi_d^1)$.

    for $i = 1, \ldots, n$ **do**

        compute: $\xi_{opt}^i = $ PO_Newt(ξ_0^i, ξ_d^i);

        set: $\xi_0^{i+1} = \xi_{opt}^i$;

    end for

Output: $\xi_{opt} = \xi_{opt}^n$.

C. Aggressive maneuver on a chicane and model validation

Virtual prototyping is the process of design, simulation, and testing of a "virtual" vehicle (i.e. a software mathematical model of a real vehicle). It allows to simulate testing maneuvers as, e.g., the ones required by international standards, thus reducing prototyping costs and time to market. Computer Aided Engineering (CAE) tools for virtual prototyping allow to create a full vehicle model so that physical and functional tests can be performed without realizing a physical prototype with a very high level of reliability. As CAE tool, we use Adams/Car developed by MSC.Software. Adams is one of the most used multibody dynamics tools in the automotive industry. A full vehicle model includes all the actual car subsystems as: steering, front and rear suspensions, chassis, front and rear tires, powertrain, brake system.

We perform an aggressive maneuver by using Adams to generate the desired curve. The objective of this choice is twofold: (i) we show the effectiveness of the exploration strategy in finding an LT-CAR trajectory close to the desired curve, and (ii) we validate the LT-CAR model by showing that the desired curve, which is a trajectory of the full Adams model, is in fact "almost" a trajectory of the LT-CAR model.

The desired curve is obtained as follows. We set as desired path the chicane depicted in Figure 6a. To obtain the desired velocity profile, we set the initial velocity to $150 km/h$ ($41.67 m/s$), and invoke an Adams routine that generates a velocity profile to drive the vehicle on the given path at maximum speed under a maximum acceleration ($\mathrm{a}_{\max}$). The remaining desired state curves are obtained by means of an Adams closed loop controller that drives

the (Adams) vehicle on the given path with the given velocity profile. The desired inputs are set to zero since they do not have an immediate correspondence with the inputs of the Adams vehicle. They are weighted lightly, thus giving the optimization the necessary freedom to track the states. With this desired trajectory in hands, to "run" the exploration strategy, we need to define the initial trajectory and the continuation update rule for the desired trajectory morphing.

The exploration strategy for this maneuver is as follows. Initially, we limit the maximum acceleration parameter to 50% of the desired one ($a_{max0} = 50\% \; a_{max}$). This gives a trajectory that can be easily projected to the LT-CAR model to get a suitable initial trajectory. Then, we increase the vehicle capabilities of a 10% acceleration step-size until the desired maximum acceleration is reached. For each intermediate step, we set the Adams trajectory as temporary desired trajectory and the optimal trajectory at the previous step as initial trajectory. A pseudo code of the strategy is given in the following table.

Algorithm 4 Exploration strategy for the chicane maneuver

Run: Adams/Car with `path` = "chicane"

    compute: velocity profile with $a_{max0} = 50\% \; a_{max}$

    run: closed-loop driver to get $\xi_d^{50\%}$

Compute: initial trajectory $\xi_0^{50\%} = \mathcal{P}(\xi_d^{50\%})$

for $i = 50, \ldots, 100$ **do**

  Run: Adams/Car with `path` = "chicane"

    compute: velocity profile with $a_{maxi} = i\% \; a_{max}$

    run: closed-loop driver to get $\xi_d^{i\%}$

  Compute: $\xi_{opt}^{i\%} = \text{PO\_Newt}(\xi_0^{i\%}, \xi_d^{i\%})$;

  Set: $\xi_0^{(i+10)\%} = \xi_{opt}^{i\%}$;

end for

Output: $\xi_{opt} = \xi_{opt}^{100\%}$.

In Figure 6 we show the results of the numerical computations. In Figure 6b a reasonably small (less than 0.2 m) path error can be observed. In Figure 6c and Figure 6d we report respectively the longitudinal and lateral speed profiles followed by the LT-CAR model versus the Adams vehicle. The maximum error is less than $0.36 m/s$ for the longitudinal speed and $0.22 m/s$ for the lateral one. Comparing Figure 6f with Figure 6c, we may notice the relationship between the load transfer and the longitudinal acceleration (velocity slope). The vehicle enters the first turn decreasing the vehicle speed (constant negative slope) and the front load suddenly increases due to the load transfer induced by the strong braking. After the first turn the velocity is slightly increased (constant positive slope) as well as the load on the rear. Entering the second turn, the vehicle reduces its speed again and then accelerates out again. It is worth noting in Figure 6f how the LT-CAR load transfer follows accurately the Adams vehicle load transfer except for a high frequency oscillation (probably due to the Adams suspensions transient). We stress the

(a) The chicane maneuver.

(b) Error path.

(c) Longitudinal velocity v_x.

(d) Lateral velocity v_y.

(e) Control inputs δ(rad) and κ(Nodim).
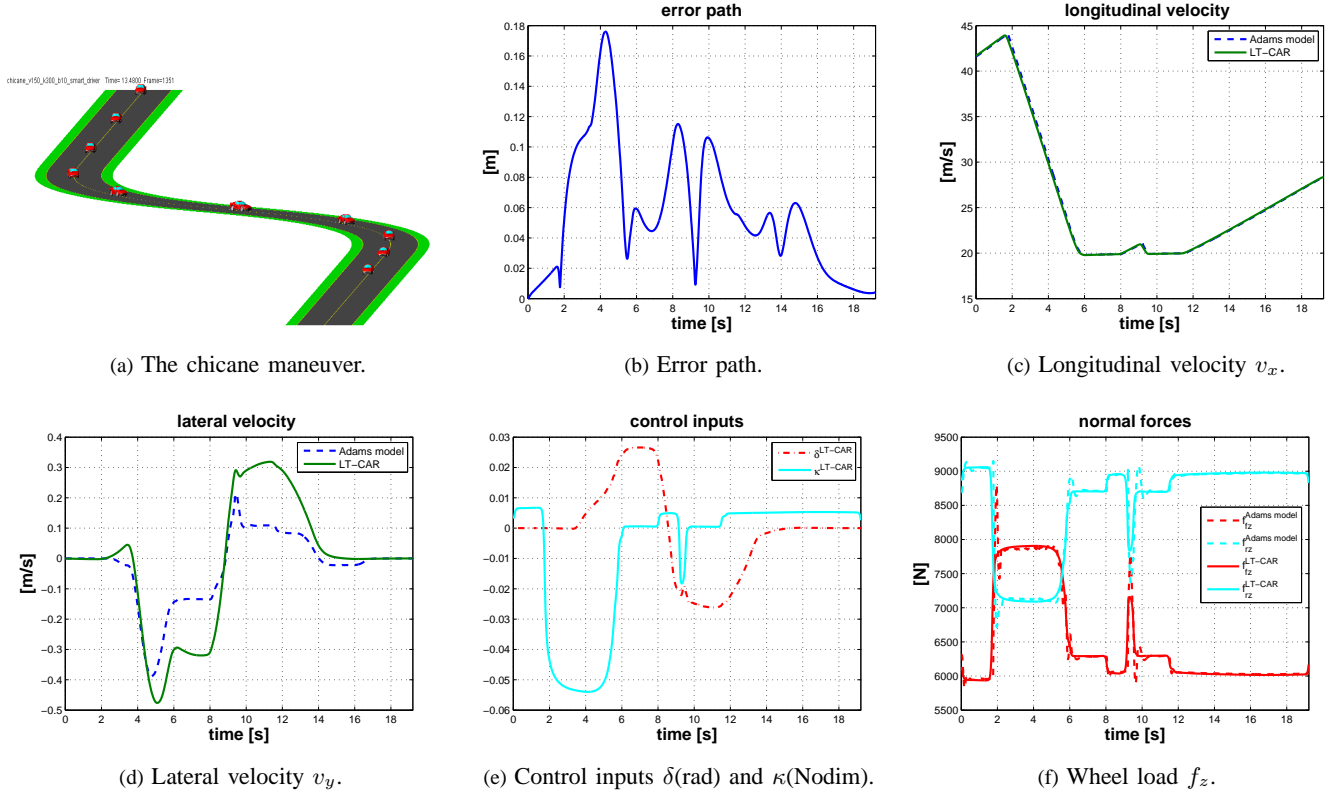
(f) Wheel load f_z.

Fig. 6: Aggressive chicane maneuver: profile of the relevant signals. The LT-CAR profiles are very close to the Adams ones.

fact that there is an accurate prediction of the load transfer although the LT-CAR has not a suspension model.

D. Constant speed maneuver on a real testing track

In this test the desired maneuver consists of following a real testing track at constant speed[1]. In particular, we choose a desired speed that in the last turn gives a lateral acceleration exceeding the tire limits. For this reason we compute the desired curve as the quasi-static trajectory of the Linear Tires LT-CAR model, $(LT)^2$-CAR, on the desired path profile depicted in Figure 7a with velocity $v = 25$m/s.

The exploration strategy for this maneuver is as follows. To morph to the desired curve, we start with a speed of 20m/s and increase the velocity profile of 1m/s at each step. For each speed value, we compute the desired curve as the quasi-static trajectory of the $(LT)^2$-CAR model on the track. As mentioned before, for the $(LT)^2$-CAR model we can always find the quasi-static trajectory. The exploration strategy thus follows the usual steps. In the following pseudo code we denote $\xi^v_{LT^2\text{-CAR}}$ the quasi-static trajectory of LT^2-CAR obtained on the given path at constant velocity v.

---

[1]See http://www.nardotechnicalcenter.com/ for details on the track

---

Algorithm 5 Exploration strategy for the constant speed maneuver

---

Given: desired path $x_d(\cdot)$, $y_d(\cdot)$ and $v_d(\cdot) \equiv 25$m/s

   compute: desired curve $\xi_d = \xi^{25\text{m/s}}_{\text{LT}^2\text{-CAR}}$;

   compute: initial trajectory $\xi^{20}_0 = \mathcal{P}(\xi^{20\text{m/s}}_{\text{LT}^2\text{-CAR}})$.

  for $v = 20, \ldots, 25$ m/s **do**

     set: $\xi^v_d = \xi^v_{\text{LT}^2\text{-CAR}}$;

     compute: $\xi^v_{opt} = \text{PO\_Newt}(\xi^v_0, \xi^v_d)$;

     set: $\xi^{v+1}_0 = \xi^v_{opt}$;

  end for

Output: $\xi_{opt} = \xi^{25}_{opt}$.

In Figures 7 the optimal trajectory of the LT-CAR model (solid green) is compared with the desired curve (dash blue) and with the optimal trajectory of the bicycle model (dash-dot red). In particular, we choose a desired speed (25m/s) that in the last turn gives a lateral acceleration exceeding the tire limits. We observe that the optimal trajectory reaches a minimum speed at the last turn, Figure 7c. Clearly increasing the desired speed increases the path error, Figure 7b.

The comparison with the classical bicycle model confirms the importance of including load transfer in the model. Indeed, the bicycle model is able to track the high speed profile much more accurately than the LT-CAR. This reveals that the bicycle model is missing important dynamic limitations due to load transfer that will appear on the real vehicle.

Next, we comment on some interesting phenomena happening in the last turn. In the first straight portion (highlighted with "1" in Figure 7a), the vehicle decelerates and moves on the right of the track to gain the most favorable position to enter the turn. Due to this fact the car is in full deceleration to face the right bend. In order to generate the required lateral forces, the tires have a high side slip angle (portion "2" in Figure 7a, see also Figure 7d). Then the car starts the exit from the turn (portion "3" in Figure 7a). With the decreasing of the centrifugal force, the lateral forces on the tires decrease, so that the longitudinal slip can increase, Figure 7f, and therefore the longitudinal forces. Thus, the car accelerates in order to regain the desired constant speed.

V. Conclusions

In this paper we studied the problem of modeling and exploring the dynamics of a single-track rigid car model that takes into account tire models and load transfer. Starting from the bicycle model, we introduced the load transfer phenomenon by explicitly imposing the holonomic constraints for the contact with the ground. The resulting model shows many of the interesting dynamic effects of a real car. For this rigid car model we characterized the equilibrium manifold and analyzed how it changes with respect to suitable parameters. Finally, we provided a set of strategies, based on nonlinear optimal control techniques and continuation methods, to explore the trajectories of the car
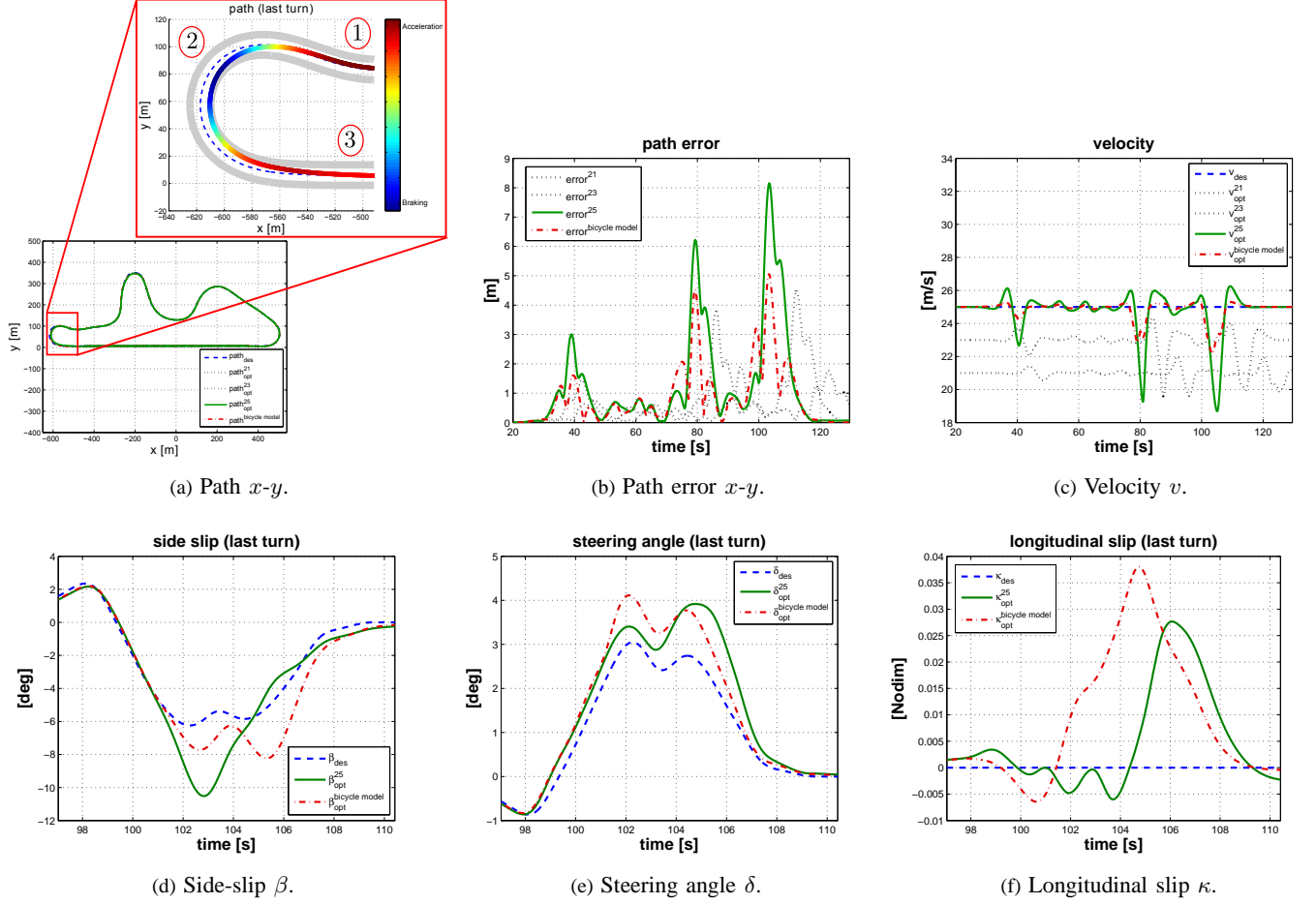
(a) Path x-y.

(b) Path error x-y.

(c) Velocity v.

(d) Side-slip β.

(e) Steering angle δ.

(f) Longitudinal slip κ.

Fig. 7: Exploration strategy for a constant speed ($25m/s$) maneuver on a real testing track. The dash, solid and dash-dot lines represent the desired curve, the optimal LT-CAR and the optimal bicycle model trajectories, respectively. Temporary optimal trajectories (for $v = 21, 23$m/s) are in light dot lines. In subplot (a) the path portion of the optimal trajectory is shown with a zoom on the last turn (entering the main straight): the corner entry ("1"), the apex point ("2"), and the corner exit ("3") are highlighted. In subplots (b) and (c) we show the path error and the velocity on the entire track. Subplots (d), (e) and (f) show the side-slip, the steering angle and the longitudinal slip in the last turn where the desired constant speed gives a desired lateral acceleration exceeding the tire limits.

model. We provided numerical computations showing the effectiveness of the exploration strategy on an aggressive maneuver and a real testing track.

APPENDIX

A. Car model parameters

The tire equations introduced in Section II-A are based on the formulation in [26]. The pure longitudinal slip is given by

$$f_{x0}(\kappa) = d_x \sin \left\{ c_x \arctan \left[b_x \kappa - e_x (b_x \kappa - \arctan b_x \kappa) \right] \right\},$$

the pure lateral slip by

$$f_{y0}(\beta) = d_y \sin\{c_y \arctan[b_y\beta - e_y(b_y\beta - \arctan b_y\beta)]\}$$

and the loss functions for combined slips by

$$g_{x\beta}(\kappa, \beta) = \cos\left[c_{x\beta}\arctan\left(\beta\frac{r_{bx1}}{1 + r_{bx2}^2\kappa^2}\right)\right],$$

$$g_{yk}(\kappa, \beta) = \cos\left[c_{yk}\arctan\left(\kappa\frac{r_{by1}}{1 + r_{by2}^2\beta^2}\right)\right].$$

The tire parameters are based on the ones given in [27].

	rear	front		rear	front
d_x	1.355	1.381	d_y	1.3	1.3
c_x	1.61	1.61	c_y	0.9	0.833
b_x	11.919	11.696	b_y	11.478	15.418
e_x	0.0263	0.0263	e_y	-2.223	-1.256
$c_{x\beta}$	1.1231	1.1231	$c_{y\kappa}$	1.0533	1.0533
r_{bx1}	13.476	13.476	r_{by1}	7.7856	7.7856
r_{bx2}	11.354	11.354	r_{by2}	8.1697	8.1697

The mass parameters are based on the ones given in [23].

Saloon car

$$m = 1150[kg] \quad a = 1.064[m] \quad b = 1.569[m] \quad h = 0.57[m]$$

$$I_b = \begin{bmatrix} 1850 & 0 & -120 \\ 0 & 1630 & 0 \\ -120 & 0 & 1850 \end{bmatrix}$$

Sports car

$$m = 1480[kg] \quad a = 1.421[m] \quad b = 1.029[m] \quad h = 0.42[m]$$

$$I_b = \begin{bmatrix} 590 & 0 & -50 \\ 0 & 1730 & 0 \\ -50 & 0 & 1950 \end{bmatrix}$$

Adams model, based on ADAMS/Car tools of *MSC.ADAMS 2005 r2* (example of four-wheeled vehicle called *MDI_Demo_Vehicle*). The tire parameters are determined by nonlinear curve-fitting routines.

	rear	front		rear	front
d_x	1.48	1.48	d_y	1.22	1.22
c_x	1.37	1.37	c_y	1.25	1.25
b_x	18.22	18.22	b_y	17.8	17.8
e_x	−0.46	−0.46	e_y	0.02	0.02
$c_{x\beta}$	1.1231	1.1231	$c_{y\kappa}$	1.0533	1.0533
r_{bx1}	13.476	13.476	r_{by1}	7.7856	7.7856
r_{bx2}	11.354	11.354	r_{by2}	8.1697	8.1697

$$m = 1528.68[kg] \quad a = 1.48[m] \quad b = 1.08[m] \quad h = 0.43[m]$$

$$I_b = \begin{bmatrix} 583.39 & 0 & -1.91 \\ 0 & 6129.12 & 0 \\ -1.91 & 0 & 6022.36 \end{bmatrix}$$

B. Reduced order model without load transfer (bicycle model)

The vector $q_r = (x, y, \psi)^T$ provides a valid set of generalized coordinates for dynamics calculations. So, the equations of motion for a Single-track rigid car with generalized coordinates $q_r = (x, y, \psi)^T$ are given by

$$\mathcal{M}_{11}(q_r)\ddot{q}_r + \mathcal{C}_1(q_r, \dot{q}_r) + \mathcal{G}_1(q_r) = \mathcal{U}_1$$

where the mass matrix is

$$\mathcal{M}_{11}(q_r) = \begin{bmatrix} m & 0 & -mbs_\psi \\ 0 & m & mbc_\psi \\ -mbs_\psi & mbc_\psi & (I_{zz} + mb^2) \end{bmatrix},$$

the Coriolis and gravity vectors are

$$\mathcal{C}_1(q_r, \dot{q}_r) = \begin{bmatrix} -mbc_\psi\dot{\psi}^2 \\ -mbs_\psi\dot{\psi}^2 \\ 0 \end{bmatrix} \quad \mathcal{G}_1(q_r) = \begin{bmatrix} 0 \\ 0 \\ 0 \end{bmatrix}$$

and the vector of generalized forces is

$$\mathcal{U}_1 = J_f^T(\psi)f = \begin{bmatrix} c_\psi & -s_\psi & c_\psi & -s_\psi \\ s_\psi & c_\psi & s_\psi & c_\psi \\ 0 & (a+b) & 0 & 0 \end{bmatrix} \begin{bmatrix} f_{fx} \\ f_{fy} \\ f_{rx} \\ f_{ry} \end{bmatrix}.$$

REFERENCES

[1] A. Rucco, G. Notarstefano, and J. Hauser, "Dynamics exploration of a single-track rigid car model with load transfer," in *IEEE Conf. on Decision and Control*, Atlanta, GA, USA, December 2010, pp. 4934–4939.

[2] T. D. Day, "An overview of the HVE vehicle model," in *SAE, paper no. 950308*, 1995, pp. 55–68.

[3] R. Frezza and A. Beghi, "A virtual motorcycle driver for closed-loop simulation," *IEEE Control Systems Magazine*, vol. 5, pp. 62–77, 2006.

[4] W. F. Milliken and D. L. Milliken, *Race car vehicle dynamics*. SAE International, 1995.

[5] T. D. Gillespie, *Fundamentals of Vehicle Dynamics*. SAE, Warrendale, 1992.

[6] J. Y. Wong, *Theory of ground vehicles*. John Wiley & Sons, 2001.

[7] U. Kiencke and L. Nielsen, *Automotive Control Systems for Engine, Driveline, and Vehicle*. Springer Verlag, 2005.

[8] R. Rajamani, *Vehicle Dynamics and Control*. Springer, 2006.

[9] E. Velenis, P. Tsiotras, and J. Lu, "Optimality properties and driver input parameterization for trail-braking cornering," *European Journal of Control*, vol. 14, no. 4, pp. 308–320, 2008.

[10] E. Velenis, E. Frazzoli, and P. Tsiotras, "Steady-state cornering equilibria and stabilization for a vehicle during extreme operating conditions," *International Journal of Vehicle Autonomous Systems*, vol. 8, no. 2–4, 2010.

[11] E. Ono, S. Hosoe, H. D. Tuan, and S. Doi, "Bifurcation in vehicle dynamics and robust front wheel steering control," *IEEE Transactions on Control Systems Technology*, vol. 6, no. 3, pp. 412–420, 1998.

[12] E. Frazzoli, "Discussion on 'Optimality properties and driver input parameterization for trail-braking cornering'," *European Journal of Control*, vol. 14, no. 4, pp. 321–324, July-August 2008.

[13] J. Yi, J. Li, J. Lu, and Z. Liu, "On the stability and agility of aggressive vehicle maneuvers: A pendulum-turn maneuver example," *IEEE Transactions on Control Systems Technology*, vol. PP, no. 99, pp. 1 –14, 2011.

[14] D. Casanova, R. Sharp, and P. Symonds, "Minimum time manoeuvring: The significance of yaw inertia," *Vehicle System Dynamics*, vol. 34, no. 2, pp. 77–115, 2000.

[15] ——, "On minimum time optimisation of formula one cars: the influence of vehicle mass," in *In Proceedings of AVEC'2000, International Symposium on Advanced Vehicle Control*, Ann Arbor, Michigan, 2000.

[16] ——, "On the optimisation of the longitudinal location of the mass centre of a formula one car for two circuits," in *In Proceedings of AVEC'2002 International Symposium on Advanced Vehicle Control*, Hiroshima, Japan, 2002.

[17] S. Anderson, S. Peters, T. Pilutti, and K. Iagnemma, "An optimal-control-based framework for trajectory planning, threat assessment, and semi-autonomous control of passenger vehicles in hazard avoidance scenarios," *International Journal of Vehicle Autonomous Systems*, vol. 8, pp. 190–216, 2010.

[18] P. Falcone, F. Borrelli, J. Asgari, H. E. Tseng, and D. Hrovat, "Predictive active steering control for autonomous vehicle systems," *IEEE Transactions on Control Systems Technology*, vol. 15, no. 3, pp. 566–580, 2007.

[19] P. Falcone, M. Tufo, F. Borrelli, J. Asgari, and H. Tseng, "A linear time varying model predictive control approach to the integrated vehicle dynamics control problem in autonomous systems," in *IEEE Conf. on Decision and Control*, New Orleans, LA, 2007, pp. 2980 – 2985.

[20] P. MacMillin and J. Hauser, "Development and exploration of a rigid motorcycle model," in *IEEE Conf. on Decision and Control*, Shanghai, China, Dec. 2009, pp. 4396–4401.

[21] A. Saccon, J. Hauser, and A. Beghi, "Trajectory exploration of a rigid motorcycle model," *IEEE Transactions on Control Systems Technology*, 2011, in press.

[22] E. L. Allgower and K. Georg, *Numerical continuation methods: an introduction*. New York, NY, USA: Springer-Verlag New York, Inc., 1990.

[23] G. Genta, *Motor vehicle dynamics: modeling and simulation*. World Scientific, 2006.

[24] J. Hauser, "A projection operator approach to the optimization of trajectory functionals," in *IFAC World Congress*, Barcelona, 2002.

[25] J. Hauser and D. G. Meyer, "The trajectory manifold of a nonlinear control system," in *IEEE Conf. on Decision and Control*, vol. 1, December 1998, pp. 1034–1039.

[26] H. B. Pacejka, *Tire and Vehicle dynamics*. Butterworth Heinemann, 2002.

[27] R. S. Sharp, S. Evangelou, and D. J. N. Limebeer, "Advances in the modelling of motorcycle dynamics," in *Multibody System Dynamics*, 2004, pp. 251–283.

[28] R. Frezza, A. Beghi, and G. Notarstefano, "Almost kinematic reducibility of a car model with small lateral slip angle for control design," in *IEEE International Symposium on Industrial Electronics*, Dubrovnik, June 2005, pp. 343–348.

[29] C. Canudas de Wit, H. Olsson, K. J. Astrom, and P. Lischinsky, "A new model for control of systems with friction," *IEEE Transactions on Automatic Control*, vol. 40(3), pp. 419–425, 1995.

[30] C. Canudas de Wit, P. Tsiotras, E. Velenis, M. Basset, and G. Gissinger, "Dynamic friction models for road/tire longitudinal interaction," *Vehicle System Dynamics*, vol. 39, no. 3, pp. 189–226, 2003.

[31] M. W. Hirsch, *Differential topology*.   Springer, New York, 1997.